



Cite this: *Soft Matter*, 2018, 14, 3572

Received 28th February 2018,
Accepted 15th April 2018

DOI: 10.1039/c8sm00406d

rsc.li/soft-matter-journal

Percolation of functionalized colloids on patterned substrates

Lucas L. Treffenstädt, ^a Nuno A. M. Araújo ^{bc} and Daniel de las Heras ^{*a}

We study the percolation properties for a system of functionalized colloids on patterned substrates via Monte Carlo simulations. The colloidal particles are modeled as hard disks with three equally-distributed attractive patches on their perimeter. We describe the patterns on the substrate as circular potential wells of radius R_p arranged in a regular square or hexagonal lattice. We find a nonmonotonic behavior of the percolation threshold (packing fraction) as a function of R_p . For attractive wells, the percolation threshold is higher than the one for clean (non-patterned) substrates if the circular wells are non-overlapping and can only be lower if the wells overlap. For repulsive wells we find the opposite behavior. In addition, at high packing fractions the formation of both structural and bond defects suppress percolation. As a result, the percolation diagram is reentrant with the non-percolated state occurring at very low and intermediate densities.

I. Introduction

Substrates patterned with space-dependent physico-chemical properties have a strong influence on the equilibrium and dynamical properties of soft materials deposited or adsorbed on them. Examples of physical processes affected by the presence of patterns include wetting,^{1,2} crystal nucleation,^{3,4} phase separation,⁵ freezing,^{6,7} adsorption,^{8,9} sedimentation,¹⁰ and colloidal transport.^{11–13}

Patterned substrates have been considered as a potential route to control the self-assembly of colloidal particles.^{14–18} For example, even simple one-dimensional periodic patterns can induce the formation of chains, regular lattices¹⁹ or even more complex structures.²⁰ In parallel, another potential route that has been considered to colloidal self-assembly is the use of particles with functionalized patches (patchy particles), yielding directional interactions and limited valence.^{21,22} Patchy colloids are ideal building blocks to obtain *e.g.* empty liquids,^{23–26} colloidal micelles,²⁷ quasicrystals,²⁸ and complex lattices.^{29,30}

The first studies of equilibrium and non-equilibrium properties of functionalized colloidal particles on substrates reveal that, even on clean (non-patterned) substrates, the critical behavior and dynamics depend strongly on the particle–particle and particle–substrate interaction and number of patches, as reviewed in ref. 31.

Here, we focus on the equilibrium properties of functionalized colloids in the presence of a patterned substrate. We consider simple patterns consisting of circular wells regularly distributed in a square or hexagonal lattice arrangement. We focus on the percolation properties and show that the critical packing fraction for percolation depends strongly on the nature of the particle–well interaction (attractive or repulsive) and on the radius of the wells, R_p . In particular, the percolation transition can either be delayed or anticipated, when compared to the critical packing fraction on a clean substrate. For a wide range of model parameters, we find a reentrant percolation transition driven by the formation of both structural and bond defects.

II. Model and methods

As summarized in Fig. 1(a), the functionalized colloidal particles are modeled as hard disks (core) of diameter $\sigma = 1$ with three patches equally distributed on their surface (perimeter). The patches are described as smaller disks of diameter $\delta/\sigma = 0.5(\sqrt{5 - 2\sqrt{3}} - 1) \approx 0.120$. The core–core interaction is hard and the patch–patch interaction is such that the potential energy decreases by ε when two patches (partially) overlap, independently of the overlapping area. For the considered size and arrangement of the patches: (i) only bonds involving two patches are possible and (ii) a pair of particles can share at most one single bond.³²

The substrate is patterned with circular wells of radius R_p with their geometric centers distributed spatially either in a square or hexagonal lattice arrangement. Particles are distributed on the substrate forming a monolayer. The particle–substrate

^a Theoretische Physik II, Physikalisches Institut, Universität Bayreuth, D-95440 Bayreuth, Germany. E-mail: delasheras.daniel@gmail.com; Web: www.danieldelasheras.com

^b Departamento de Física, Faculdade de Ciências, Universidade de Lisboa, P-1749-016 Lisboa, Portugal

^c Centro de Física Teórica e Computacional, Universidade de Lisboa, P-1749-016 Lisboa, Portugal

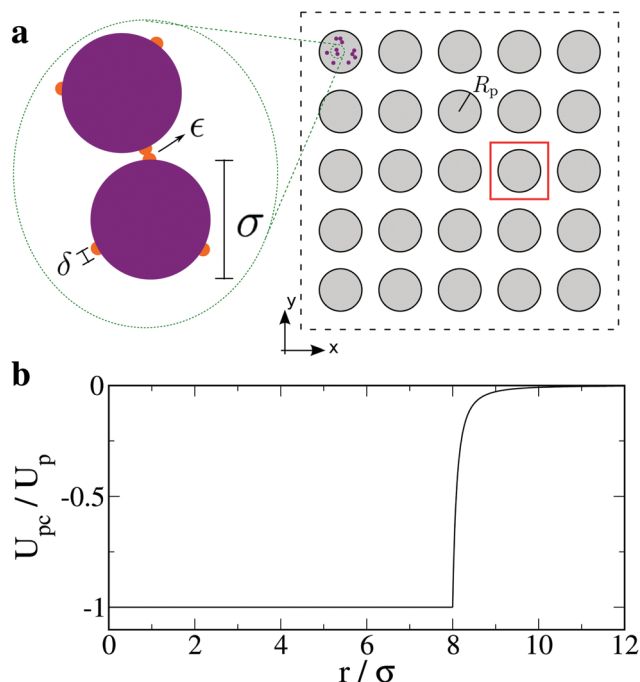


Fig. 1 (a) Schematic of the model: a substrate patterned with a square lattice of potential wells (grey circles of radius R_p). The inset shows a close view of the particle model. Colloidal particles are described as hard-core disks of diameter σ decorated with three patches (disks of diameter δ) equally distributed on their surface. Whenever two patches overlap the potential energy decreases by ϵ . The interaction potential between the wells and the colloidal particles (disks) is either attractive or repulsive. In the case of attractive wells, the particles are more likely to be found inside the wells, as illustrated in the figure. The red square symbolizes one unit cell of the pattern (the lattice constant is fixed to 20σ). Several patterns with $R_p/\sigma \in [0,15]$ are considered. (b) Plot of the radial dependence of the particle–well potential as a function of the distance r between the center of the particle and the center of the well.

interaction potential, $U_{pc}(r)$, is radial, solely depending on r , the distance between the center of the particle and the center of the well. $U_{pc}(r)$ is constant for a core $r < R_p$ and goes to zero with the inverse square distance for $r > R_p$, see Fig. 1(b). For numerical simplicity, we introduce a cut-off distance, R_c , which is fixed at half of the lateral length of the simulation box. The potential $U_{pc}(r)$ is slightly shifted such that it is continuous at R_c , so

$$\frac{U_{pc}(r)}{U_p} = \begin{cases} -1 & \text{if } r < R_p \\ 0 & \text{if } r > R_c \\ -\frac{a^2}{(r+a-R_p)^2} + \frac{a^2}{(R_c+a-R_p)^2} \frac{r-R_p}{R_c-R_p} & \text{otherwise.} \end{cases} \quad (1)$$

The parameter a controls the softness of the potential and we fix it at $a/\sigma = 0.2$. The depth of the potential well is given by U_p . We set $U_p/\epsilon = -4$ ($U_p/\epsilon = 4$) for the case of repulsive (attractive) potential wells. We consider 25 and 36 wells for square and hexagonal lattices, respectively. For both hexagonal and square patterns the lattice constant is fixed to 20σ . Thus, the lateral length of the substrate is $L \approx 100\sigma$ and two potential wells

overlap if $R_p/\sigma \geq 10$. Whenever two or more wells overlap, the potential inside the overlapping region is always set to U_p . We consider several sizes of the wells in the range $R_p/\sigma \in [0,15]$ which goes from very small ($R_p \approx \sigma$) non-overlapping wells to very large ($R_p \gg \sigma$) fully overlapping wells. We use periodic boundary conditions along both directions.

We performed canonical Monte Carlo simulations to study the percolation properties. The control parameter is the packing fraction, $\eta = Nv_0/A$, where N is the number of particles, $v_0 = \pi(\sigma/2)^2$ is the volume (area) of the hard cores, and A is the total area of the substrate. Here, we consider values of N in the range $\approx [10^3, 10^4]$, and thus $\eta \approx [0.1, 0.7]$. At each Monte Carlo sweep (MCS), we sequentially perform an attempt to move and rotate every particle. The displacements and the rotation angles are randomly generated from a uniform distribution. At the beginning of each simulation we estimate the maximum displacement and maximum rotation angle that each particle is allowed to perform in one move. Both parameters are adjusted such that approximately 50% of all particles moves are accepted during the simulation.

To generate the initial configuration, we distribute the particles without overlapping and then run 10^4 MCS at a very high temperature ($k_B T/\epsilon = 10^2$) such that the positions and the orientations of all particles are randomized. We then equilibrate the system running 5×10^6 – 10^7 MCS (depending on the model parameters) and accumulate data over 10^6 – 10^7 additional MCS.

III. Results

In bulk, a two-dimensional system of functionalized particles with three patches undergoes a first order vapor–liquid transition by increasing the density at sufficiently low temperatures.³² The transition line ends at a critical point for high temperatures. Above the critical temperature, a continuous percolation transition is still observed by increasing the particle density.

Here, to focus on the role of the pattern, we fix the temperature at $k_B T/\epsilon = 0.15$, which is well above the vapor–liquid critical point of the bulk phase diagram.³² We first analyze the percolation transition on a clean substrate, *i.e.*, a substrate with no potential wells. To characterize the percolation transition, we measure the fraction \bar{s} of particles belonging to the largest cluster of connected particles. For simplicity, we estimate the percolation threshold as the value of the packing fraction $\eta = \eta_0$ at which $\bar{s} = 1/2$. As shown in Fig. 2(a), this roughly coincides with the position of the peak in the second moment of the cluster-size distribution. We estimate $\eta_0 \approx 0.33$ for a clean substrate. Snapshots for packing fractions below, close, and above the percolation threshold are shown in Fig. 2(b). Fig. 2(c) shows the cluster-size distribution $P(s)$, where s is the fraction of particles in the cluster. At low packing fractions the particles are aggregated in small (finite) clusters, while above the percolation threshold, there is an infinite cluster that spans the entire substrate.

A. Percolation on a patterned substrate: square lattice

Let us first consider a pattern consisting of attractive circular wells arranged in a square lattice. Fig. 3 shows the cluster-size

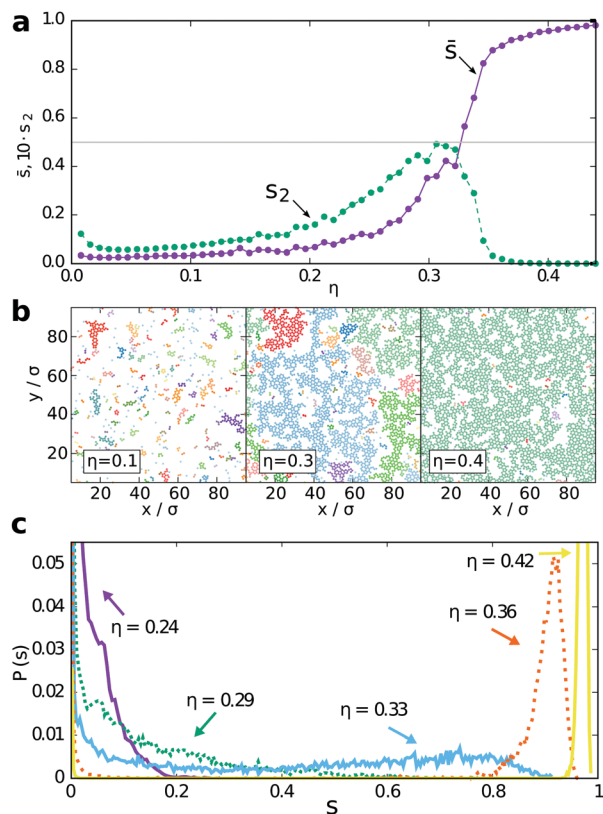


Fig. 2 Percolation on a clean substrate. (a) Fraction of particles in the largest cluster \bar{s} and second moment of the cluster-size distribution s_2 (multiplied by a factor 10 for visualization purposes) as a function of the packing fraction. (b) Snapshots for three packing fractions: below $\eta = 0.1$ (left), close to $\eta = 0.3$ (middle), and above $\eta = 0.4$ (right) the percolation transition. Each cluster is colored differently. (c) Cluster size distribution $P(s)$, as a function of the cluster size s , for different values of the packing fraction, as indicated.

distribution, $P(s)$, for different packing fractions, when the radius of the wells is $R_p/\sigma = 8$. Clearly, $P(s)$ is significantly different from the one obtained on a clean substrate, see Fig. 2(c). $P(s)$ is

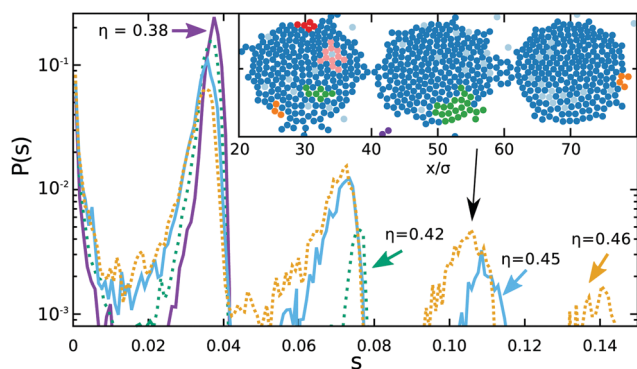


Fig. 3 Semi-logarithmic plot of the cluster-size distribution $P(s)$ as a function of the cluster size s for different values of the packing fraction, as indicated. The substrate is patterned with a square lattice of circular potential wells of radius $R_p/\sigma = 8$. The inset is a partial snapshot of the simulation box ($\eta = 0.45$) showing a cluster of colloidal particles that extends over three potential wells. Different particle colors correspond to different clusters.

characterized by a sequence of well defined peaks for cluster of sizes $s \approx ns_0$. Here, s_0 is the characteristic size of a cluster of radius R_p and $n = 1, 2, 3, \dots$. As shown in the inset of Fig. 3, the colloidal particles tend to accumulate inside the attractive wells, what promotes the formation of compact clusters. As the average packing fraction increases, not all particles can fit within the potential well and thus they occupy the interstitials between the wells. Nevertheless, since the particle–well interaction potential decays with the distance to the center, the particles tend to accumulate close to the perimeter defined by R_p . For repulsive wells, the colloidal particles tend first to occupy the interstitials and only for high average packing fractions occupy the core of the wells.

Fig. 4 summarizes our findings for the percolation properties on a substrate with potential wells organized in a square lattice. Fig. 4(a) is the two-parameter percolation diagram (packing fraction η vs. radius of the well R_p), for attractive (right-hand side) and repulsive (left-hand side) wells. The system exhibits a very rich behavior that we discuss in detail below.

Attractive wells. We start describing the limit of small non-overlapping attractive wells. In this case, the colloidal particles tend to accumulate inside the wells. Only when the density inside the wells is significantly high, particles occupy the space in between wells, eventually forming bridges between clusters in different wells, what leads to global percolation. Therefore, the packing fraction at the percolation threshold, η_p , is larger than the one for clean substrates η_0 .

To characterize the structure of the clusters, we calculate the orientational order parameter

$$\tilde{q}_6^{(i)} = \left| \frac{1}{6} \sum_{j=1}^{n_i} \exp(i6\theta_j^{(i)}) \right|, \quad (2)$$

where, $\theta_j^{(i)}$ is the angle between an arbitrary axis of reference and the vector joining the geometrical centers of particles i and j . The sum runs over all particles at a distance $r/\sigma < 1.2$ from particle i . This order parameter is one when particle i is surrounded by six neighbors in a hexagonal configuration.

Snapshots below and above the percolation transition in the case of small non-overlapping wells are shown in Fig. 4(b), state points 0 and 1, respectively. (See also Fig. 4(a) to locate the state points in the percolation diagram.) The particles are colored according to their order parameter \tilde{q}_6 .

At the percolation transition, the particle density inside the wells is much higher than the percolation density on a clean substrate. Inside the wells, particles are organized in a six-fold symmetry, corresponding to a high value of the order parameter \tilde{q}_6 . However, not all patches are bonded due to geometrical constraints. At very high packing fractions, particles in the largest, percolated cluster are fully bonded, forming a honeycomb-like lattice with an isolated (not bonded) particle in the middle, as shown in the inset of Fig. 4(b), for the state point 3. In the interstitials of the wells, the particles form an open network (note the low value of \tilde{q}_6), similar to what is observed for clean substrates close to the percolation threshold.

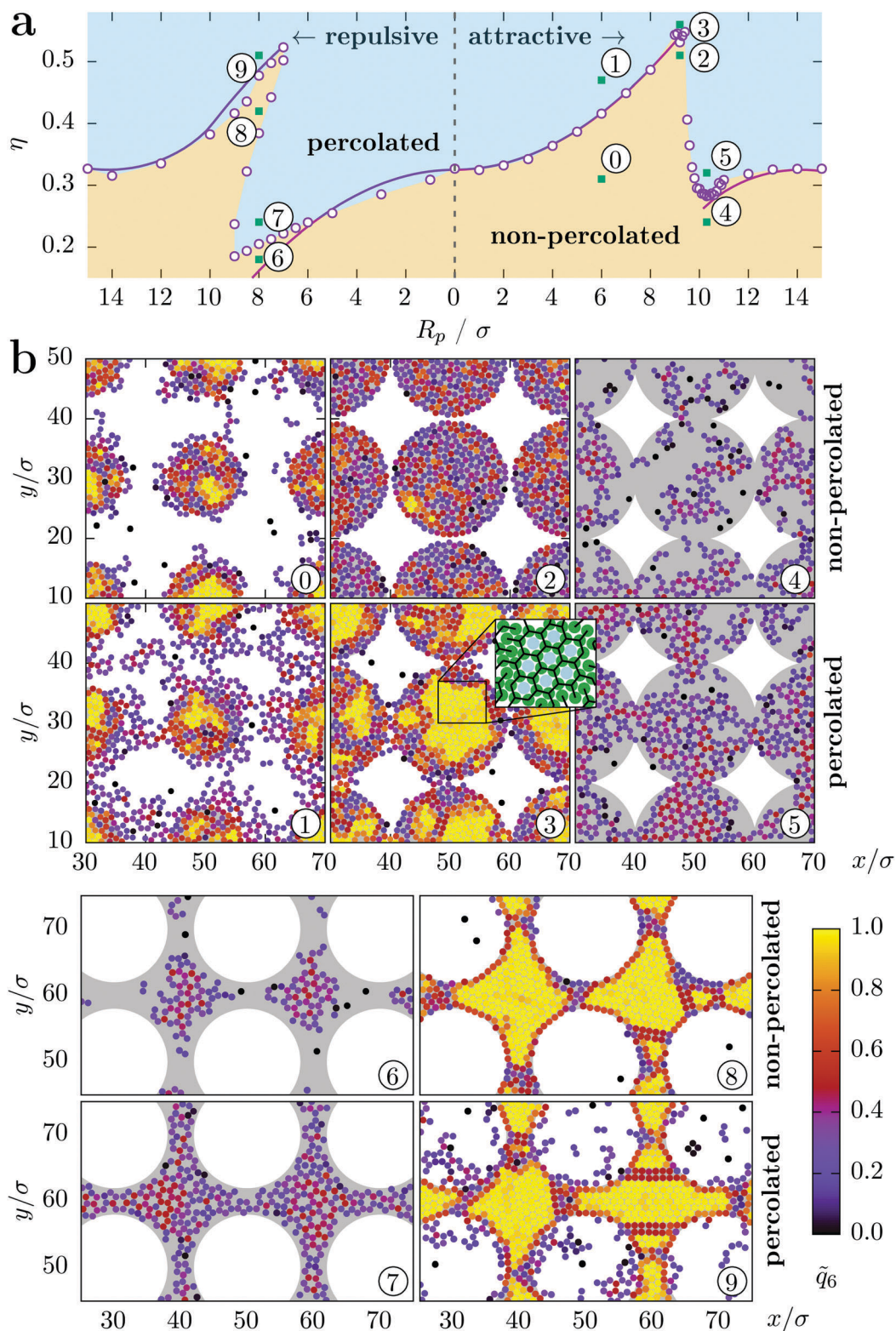


Fig. 4 Square lattice. (a) Percolation phase diagram in the plane of radius of the potential well core R_p and packing fraction η . The light brown (light blue) area is the non-percolated (percolated) region, as indicated. On the left (right) of the vertical dashed line, we show the results for repulsive (attractive) wells. The wells on the substrate form a square lattice. The numbered green squares are selected state points for which a snapshot is shown in panel (b). The empty circles are the percolation values estimated numerically using Monte Carlo simulations. The solid line is the theoretical prediction (see text for details). (b) Selected snapshots of the central region of the substrate. The packing fractions and radii of the well of each configuration is indicated in panel (a) (green squares). The top (bottom) group of snapshots correspond to attractive (repulsive) wells. The grey areas indicate the energetically favorable regions for the colloidal cores. The colloids are colored according to the value of their order parameter \tilde{q}_6 . The inset in the snapshot 3 is a close view showing the underlying bonding lattice: a honeycomb lattice with an isolated particle in each unit cell.

Based on the observations described above, we can estimate the packing fraction at the percolation threshold. For that, we hypothesize that (i) the packing fraction inside the wells is $\eta_1 > \eta_0$; (ii) the packing fraction in the interstitials is the same as the one for a clean substrate, η_0 . Hence, the percolation threshold, for non-overlapping attractive wells is

$$\eta_{a,\text{no}}(R_p) = A_{\text{no}}\eta_1 + (1 - A_{\text{no}})\eta_0, \quad (3)$$

where A_{no} is the fraction of the area of the substrate covered by the core of the wells (within R_p). Thus, for non-overlapping wells, $A_{\text{no}} = n_p \pi R_p^2 / A$, with n_p the number of wells and A the area of the substrate. As shown in Fig. 4(a) (solid lines), eqn (3) with $\eta_1 = 0.65$ is a good estimator for the percolation line. In the limit $A_{\text{no}} \rightarrow 0$ (very-small wells), the packing fraction at the percolation threshold converges to the one on a clean substrate, *i.e.*,

$$\lim_{R_p \rightarrow 0} \eta_p(R_p) = \eta_0. \quad (4)$$

The packing fraction at the percolation threshold increases monotonically with R_p until $R_p/\sigma \approx 9$. For this value of R_p , $\eta_p \approx 0.54$, which is about 1.6 times higher than the one on a clean substrate. Above that value of R_p , an abrupt decay of η_p is observed. From $R_p/\sigma \approx 9.4$ to $R_p/\sigma \approx 10.2$ the packing fraction changes from $\eta_p \approx 0.54 > \eta_0$ to $\eta_p \approx 0.28 < \eta_0$. For our setup, the lattice constant of the pattern is 20σ . Hence, the core of two neighboring wells mutually overlap if $R_p \geq R_t$, with $R_t/\sigma = 10$. Therefore, if the well radius is $R_p \geq R_t - \sigma - 2\delta \approx 9\sigma$, it is possible to have bonds between particles inside two different wells. See the snapshots shown in Fig. 4(b) state points 2 (non-percolated) and 3 (percolated). This is the reason behind the abrupt decay of η_p .

If the core of the wells overlaps, a percolation cluster can be formed by particles all inside the core of the wells. As a result, the packing fraction at the percolation transition decreases with respect to that on a clean substrate. Also in this limit, it is possible to estimate the percolation threshold. For that, we hypothesize that (i) the particles are all within the core of the wells; (ii) the packing fraction inside the wells is η_0 . Then, the percolation transition is expected to occur at,

$$\eta_{a,o}(R_p) = A_o\eta_0, \quad (5)$$

where A_o is the area fraction of the substrate covered by overlapping wells. A comparison between the predicted packing fraction and the simulation results is shown in Fig. 4(a). Snapshots below and above the percolation threshold for the case of overlapping wells are shown in Fig. 4(b), state points 4 and 5, respectively. The minimum threshold is obtained for $R_p/\sigma \approx 10.2$, for which $\eta_p \approx 0.28$, what is $\sim 15\%$ lower than the one on a clean substrate.

If the wells are very large, in comparison to the particle size, then the entire substrate is covered by cores of the wells and the potential is uniform across the substrate. In this limit, $A_o \rightarrow 1$, and we recover the percolation threshold on a clean substrate, *i.e.*,

$$\lim_{R_p \gg \sigma} \eta_p(R_p) = \eta_0. \quad (6)$$

Repulsive patches. The percolation phase diagram for a square lattice of repulsive patches is shown in the left-hand side of Fig. 4(a). The wells and the interstitials interchange their

role with respect to the case of attractive wells. The wells are repulsive and hence the colloidal particles tend to occupy first the interstitials until the density there is very high. The limit of small repulsive wells is similar to the limit of very large attractive wells. In both cases, we find $\eta_p < \eta_0$. The snapshots 6 and 7, in Fig. 4(b), correspond to a non-percolated and a percolated state, respectively, in the regime of non-overlapping repulsive wells. To predict the percolation threshold for non-overlapping repulsive wells, we hypothesize that (i) the particles completely avoid the repulsive wells; (ii) in the interstitials the packing fraction is the same as in a clean substrate. Then,

$$\eta_{r,\text{no}} = (1 - A_{\text{no}})\eta_0. \quad (7)$$

This simple geometrical model slightly overestimates the effect of the substrate on the transition (see Fig. 4(a)), but still provides a qualitative description of the percolation line. Note that, the above hypotheses are valid only in the limit of a very strong substrate-particle interaction, in which the particles completely avoid the repulsive regions.

The packing fraction at the percolation threshold decreases monotonically with R_p until $R_p/\sigma \approx 9$. For wells of size $R_p/\sigma = 9$, the percolation transition occurs at $\eta_p \approx 0.19$, that is $\sim 45\%$ lower than on a clean substrate.

In the limit of large repulsive wells, particles tend to accumulate in the interstitials, which are now isolated. This limit corresponds to what is observed for small attractive wells. Therefore, as discussed above, to form a percolation cluster, it is necessary to form bridges between interstitials. The larger the interstitials are (without overlapping), the higher the packing fraction is at the percolation threshold. An estimation for the packing fraction at the percolation threshold is given by,

$$\eta_{r,o} = (1 - A_o)\eta_1 + A_o\eta_0. \quad (8)$$

To obtain this expression, we assumed that, at the percolation threshold, the density in the interstitials is η_1 and the density inside the repulsive wells is η_0 . As before, setting $\eta_1 = 0.65$, we obtain a good qualitative and quantitative agreement with the numerical data, see Fig. 4(a).

We find a reentrant percolation transition for repulsive wells of size $7 \lesssim R_p/\sigma \lesssim 9$, see Fig. 4(a). By increasing the packing fraction (vertical direction in the diagram), we find: non-percolated, percolated, non-percolated, percolated states. The snapshots 6, 7, 8, and 9 in Fig. 4(b), are representative of the reentrant transition. The percolation at low packing fractions (state points 6 and 7) corresponds to the one on a substrate of non-overlapping repulsive wells, where particles accumulate in the interstitials. Surprisingly, by increasing the packing fraction, the system undergoes a transition from a percolated to a non-percolated state (see state points 7 and 8). This transition is driven by the formation of defects on both the orientational and the spatial order of the particles. To accommodate an increase in the density of particles in the interstitials, the particles organize in a compact manner, with local hexagonal order, as indicated by the high value of \tilde{q}_c (state points 8 and 9). The particles form also a fully bonded honeycomb-like structure with isolated particles in the middle of each unit cell. As shown

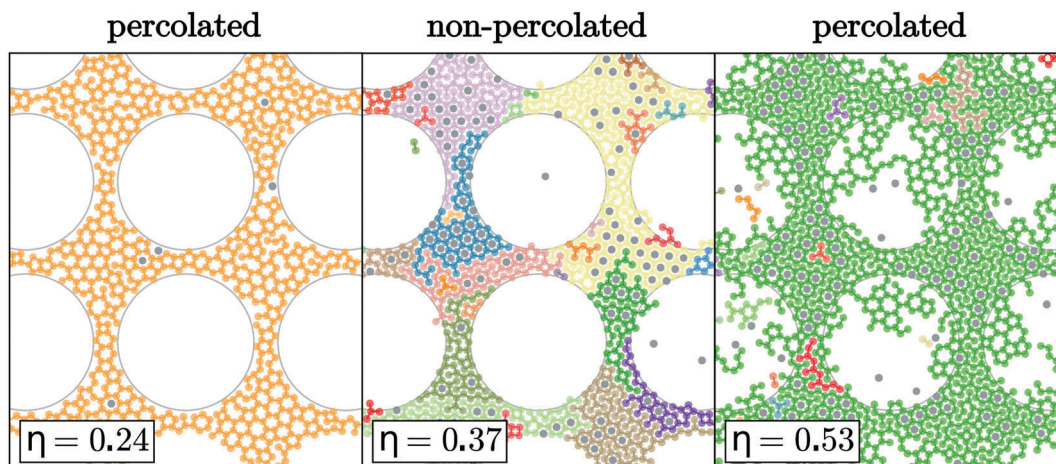


Fig. 5 Snapshots (partial region) for three different packing fractions, as indicated. The substrate is patterned with a square lattice of circular repulsive wells of radius $R_p/\sigma = 8$. An arbitrary color has been assigned to each cluster. The system undergoes a reentrant percolation transition by increasing the packing fraction.

in Fig. 4(b) and 5, the interstitials are interconnected through narrow channels, with a width of a few particle diameters. Through these channels, the formation of a percolation cluster might be suppressed due to the emergence of bond and structural defects. A local drop of the order parameter \bar{q}_6 signals the position of the structural defects, see state points 8 and 9. The bond defects are visible in the snapshots shown in Fig. 5, where different clusters have different colors. For even larger packing

fractions, the percolation is recovered *via* the formation of bridges inside the repulsive wells, see state point 9, in Fig. 4(b).

In Fig. 6, we show the fraction of particles in the largest cluster (a) and the second moment of the cluster-size distribution (b) in a substrate with repulsive wells of $R_p/\sigma = 8$. Both quantities are consistent with a reentrant transition. We have considered different system sizes and no strong finite-size effects are observed (see figure).

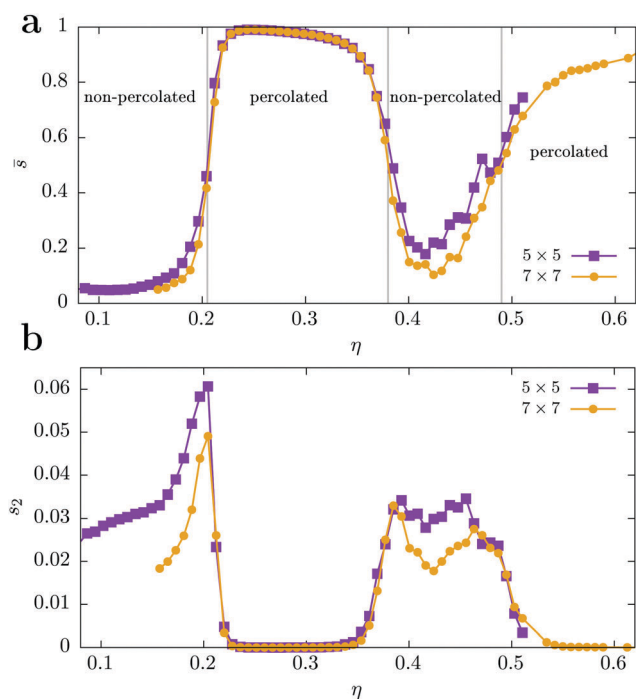


Fig. 6 Fraction of particles in the largest cluster (a) and second moment of the cluster-size distribution (b) as a function of the packing fraction. The substrate consists of a square lattice of $n_p \times n_p$ repulsive wells, each of size $R_p/\sigma = 8$. Two system sizes are shown: $n_p = 5$ (violet squares) and $n_p = 7$ (orange circles). The gray vertical lines in (a) indicate the packing fraction at which $\bar{s} = 0.5$, what roughly coincides with the maximum in s_2 .

B. Percolation on a patterned substrate: hexagonal lattice

We now consider a pattern consisting of circular wells arranged in a hexagonal lattice. The percolation phase diagram together with snapshots are shown in Fig. 7(a) and (b), respectively.

The percolation phase diagram is qualitatively the same as in the case of a square lattice. The simple geometrical models also predicts quantitatively the packing fraction at the percolation transition. The reentrant percolation transition for repulsive wells is also observed. As in the previous substrate pattern, the formation of defects drives a transition to a non-percolated state by increasing the density from a percolated state.

IV. Summary and conclusions

The presence of a patterned substrate substantially affects the percolation properties of a system of functionalized colloidal particles. We have studied substrate patterns consisting of a sequence of either attractive or repulsive circular wells. For increasing packing fractions, the colloidal particles accumulate first in the regions of lower potential energy, *i.e.*, inside the wells if they are attractive or in between if they are repulsive. The regions of high potential energy are only occupied for large packing fractions. When the regions of lower potential energy percolate (*e.g.* overlapping attractive wells), the percolation transition for the colloidal particles occurs for lower packing fractions than in the case of a clean (non-patterned) substrate. On the contrary, if the low potential energy regions are fragmented, the percolation threshold is indeed larger than in a clean substrate.

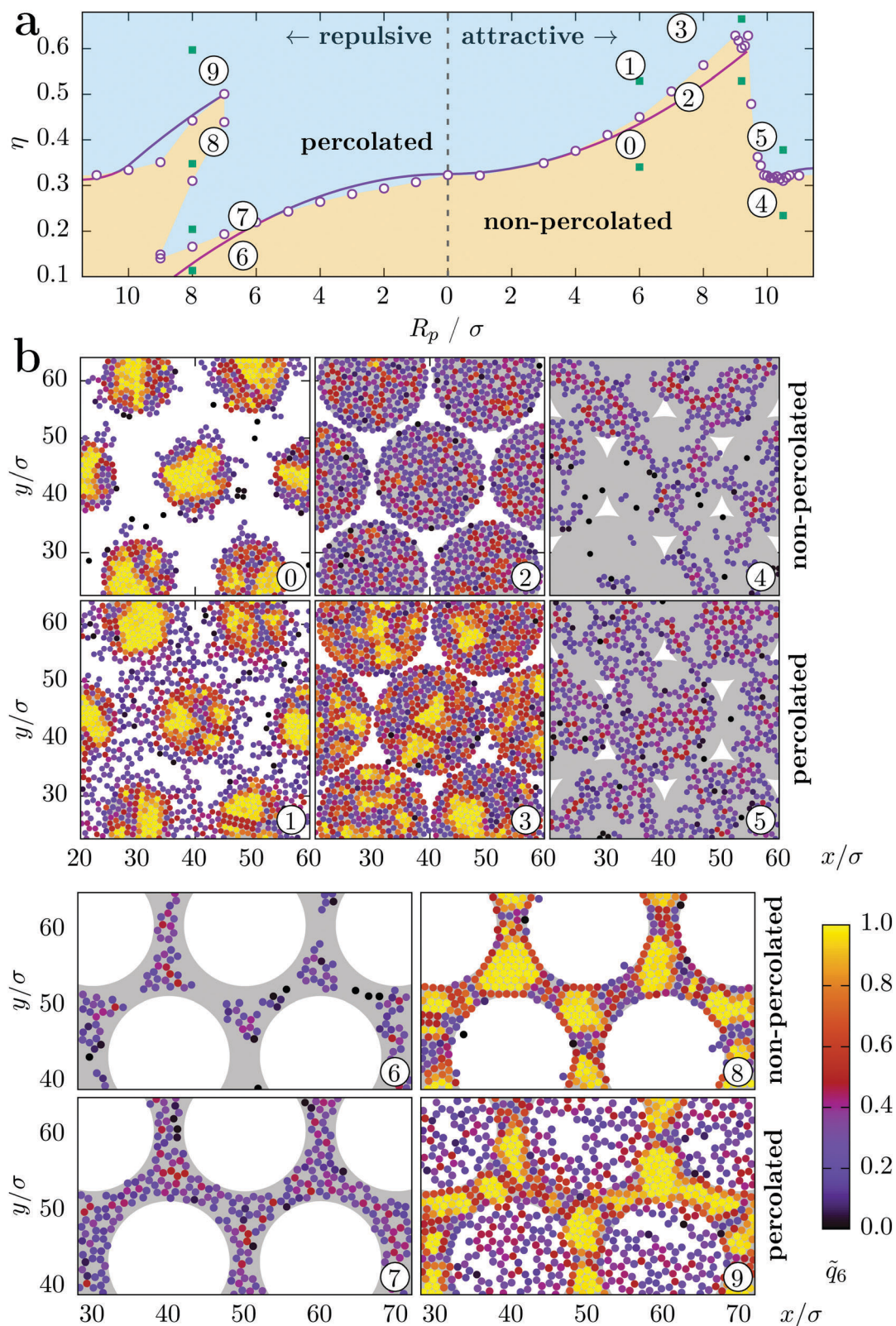


Fig. 7 Hexagonal lattice. (a) Percolation phase diagram in the plane of radius of the potential well core R_p and packing fraction η . The light brown (light blue) area is the non-percolated (percolated) region, as indicated. On the left (right) of the vertical dashed line we show the results for repulsive (attractive) wells. The wells on the substrate form a hexagonal lattice. The numbered green squares are selected state points for which a snapshot is shown in panel (b). The empty circles are the percolation values estimated numerically using Monte Carlo simulations. (b) Selected snapshots of the central region of the substrate. The packing fractions and radii of the well of each configuration is indicated in panel (a) (green squares). The top (bottom) group of snapshots correspond to attractive (repulsive) wells. The grey areas indicate the energetically favorable regions for the colloidal cores. The colloids are colored according to the value of their order parameter \tilde{q}_6 .

We have shown that the percolation threshold can be estimated by a simple model, based on pure geometric arguments.

In the case of repulsive wells, we find a reentrant percolation transition related to the formation of structural and bond defects, what suppresses percolation for intermediate values of packing fraction. The percolation is only recovered for very high packing fractions. Previous studies of functionalized colloidal particles have reported also reentrant phenomena driven by, *e.g.*, gravitational fields,^{33,34} competition between different energy scales,^{35–37} and patches activated by temperature.³⁸

For non-overlapping wells, the cluster-size distribution is characterized by well-defined peaks at certain cluster sizes. This suggests that the percolation transition might be no longer continuous.³⁹ Future works might consider studying the nature of the transition in detail for different patterns, temperatures, and number of patches per particle.

For simplicity, we considered a two-dimensional system but we expect the results to be valid in the sub-monolayer regime, provided that the vertical position of the particles relative to the substrate does not vary significantly. There are several experimental techniques available to obtain patterned substrates, such as, *e.g.*, microcontact printing,⁴⁰ chemically patterned substrates with anionic and cationic regions,⁴¹ soft lithography,⁴² and optical substrates using arrays of optical tweezers.^{43–46} Also various approaches have been developed to synthesize functionalized colloids.^{22,47–50}

We have considered a monocomponent system. New phenomenology is expected in the case of binary and ternary mixtures of functionalized colloids for which several types of percolated states are possible. Examples are bigels^{51,52} and trigels⁵³ in which interpenetrated networks made of single species percolate the system.

Finally, we have focused on equilibrium properties. Some of the phenomenology described here might be dynamically inaccessible due to the formation of kinetically trapped structures.^{9,31,54,55} Analyzing the dynamics on patterned substrates is therefore a fundamental question of practical interest that should be considered in future works.

Conflicts of interest

There are no conflicts of interest to declare.

Acknowledgements

This work was partially funded by the Portuguese-German FCT/DAAD project “Self-organization of colloidal particles on patterned substrate” (DAAD project-id: 57339919). NA also thanks financial support from the Portuguese Foundation for Science and Technology (FCT) under the contract no. UID/FIS/00618/2013.

References

- 1 P. Lenz and R. Lipowsky, *Phys. Rev. Lett.*, 1998, **80**, 1920.
- 2 C. Bauer and S. Dietrich, *Phys. Rev. E: Stat. Phys., Plasmas, Fluids, Relat. Interdiscip. Top.*, 1999, **60**, 6919.
- 3 J. Aizenberg, A. J. Black and G. M. Whitesides, *Nature*, 1999, **398**, 495.
- 4 T. Neuhaus, M. Schmiedeberg and H. Löwen, *New J. Phys.*, 2013, **15**, 073013.
- 5 M. Böltau, S. Walheim, J. Mlynek, G. Krausch and U. Steiner, *Nature*, 1998, **391**, 877.
- 6 M. Heni and H. Löwen, *Phys. Rev. Lett.*, 2000, **85**, 3668.
- 7 W.-S. Xu, Z.-Y. Sun and L.-J. An, *J. Chem. Phys.*, 2010, **132**, 144506.
- 8 N. A. M. Araújo, A. Cadilhe and V. Privman, *Phys. Rev. E: Stat., Nonlinear, Soft Matter Phys.*, 2008, **77**, 031603.
- 9 N. A. M. Araújo, C. S. Dias and M. M. Telo da Gama, *J. Phys.: Condens. Matter*, 2017, **29**, 014001.
- 10 I. B. Ramsteiner, K. E. Jensen, D. A. Weitz and F. Spaepen, *Phys. Rev. E: Stat., Nonlinear, Soft Matter Phys.*, 2009, **79**, 011403.
- 11 P. Tierno and T. M. Fischer, *Phys. Rev. Lett.*, 2014, **112**, 048302.
- 12 J. Loehr, M. Loenne, A. Ernst, D. de las Heras and T. M. Fischer, *Nat. Commun.*, 2016, **7**, 11745.
- 13 J. Loehr, D. de las Heras, A. Jarosz, M. Urbaniak, F. Stobiecki, A. Tomita, R. Huhnstock, I. Koch, A. Ehresmann, D. Holzinger and T. M. Fischer, *Commun. Phys.*, 2018, **1**, 4.
- 14 Q. Guo, C. Arnoux and R. E. Palmer, *Langmuir*, 2001, **17**, 7150.
- 15 K. M. Chen, X. Jiang, L. C. Kimerling and P. T. Hammond, *Langmuir*, 2000, **16**, 7825.
- 16 N. Vogel, M. Retsch, C.-A. Fustin, A. del Campo and U. Jonas, *Chem. Rev.*, 2015, **115**, 6265.
- 17 D. Wang and H. Mohwald, *J. Mater. Chem.*, 2004, **14**, 459.
- 18 A. Cadilhe, N. A. M. Araújo and V. Privman, *J. Phys.: Condens. Matter*, 2007, **19**, 065124.
- 19 Y.-H. Ye, S. Badilescu, V.-V. Truong, P. Rochon and A. Natansohn, *Appl. Phys. Lett.*, 2001, **79**, 872.
- 20 H. M. Harreis, M. Schmidt and H. Löwen, *Phys. Rev. E: Stat., Nonlinear, Soft Matter Phys.*, 2002, **65**, 041602.
- 21 E. Bianchi, R. Blaak and C. N. Likos, *Phys. Chem. Chem. Phys.*, 2011, **13**, 6397.
- 22 Y. Wang, Y. Wang, D. R. Breed, V. N. Manoharan, L. Feng, A. D. Hollingsworth, M. Weck and D. J. Pine, *Nature*, 2012, **491**, 51.
- 23 E. Bianchi, J. Largo, P. Tartaglia, E. Zaccarelli and F. Sciortino, *Phys. Rev. Lett.*, 2006, **97**, 168301.
- 24 D. de las Heras, J. M. Tavares and M. M. Telo da Gama, *J. Chem. Phys.*, 2011, **134**, 104904.
- 25 D. de las Heras, J. M. Tavares and M. M. Telo da Gama, *Soft Matter*, 2011, **7**, 5615.
- 26 B. Ruzicka, E. Zaccarelli, L. Zulian, R. Angelini, M. Sztucki, A. Moussad, T. Narayanan and F. Sciortino, *Nat. Mater.*, 2011, **10**, 56.
- 27 D. J. Kraft, R. Ni, F. Smallenburg, M. Hermes, K. Yoon, D. A. Weitz, A. van Blaaderen, J. Groenewold, M. Dijkstra and W. K. Kegel, *Proc. Natl. Acad. Sci. U. S. A.*, 2012, **109**, 10787.
- 28 E. Slyk, W. Rzesko and P. Bryk, *Soft Matter*, 2016, **12**, 9538.
- 29 Q. Chen, S. C. Bae and S. Granick, *Nature*, 2011, **469**, 381.
- 30 Z. Zhang, A. S. Keys, T. Chen and S. C. Glotzer, *Langmuir*, 2005, **21**, 11547.

- 31 C. S. Dias, N. A. M. Araújo and M. M. Telo da Gama, *Adv. Colloid Interface Sci.*, 2017, **247**, 258.
- 32 J. Russo, P. Tartaglia and F. Sciortino, *Soft Matter*, 2010, **6**, 4229.
- 33 D. de las Heras, L. L. Treffenstädt and M. Schmidt, *Phys. Rev. E*, 2016, **93**, 030601.
- 34 T. Geigenfeind and D. de las Heras, *J. Phys.: Condens. Matter*, 2017, **29**, 064006.
- 35 J. Russo, J. M. Tavares, P. I. C. Teixeira, M. M. Telo da Gama and F. Sciortino, *Phys. Rev. Lett.*, 2011, **106**, 085703.
- 36 Y. V. Kalyuzhnyi and P. T. Cummings, *J. Chem. Phys.*, 2013, **139**, 104905.
- 37 S. Roldán-Vargas, F. Smalenburg, W. Kob and F. Sciortino, *J. Chem. Phys.*, 2013, **139**, 244910.
- 38 D. de las Heras and M. M. Telo da Gama, *J. Phys.: Condens. Matter*, 2016, **28**, 244008.
- 39 N. A. M. Araújo and H. J. Herrmann, *Phys. Rev. Lett.*, 2010, **105**, 035701.
- 40 A. Kumar, N. L. Abbott, H. A. Biebuyck, E. Kim and G. M. Whitesides, *Acc. Chem. Res.*, 1995, **28**, 219.
- 41 J. Aizenberg, P. V. Braun and P. Wiltzius, *Phys. Rev. Lett.*, 2000, **84**, 2997.
- 42 F. Fan and K. J. Stebe, *Langmuir*, 2004, **20**, 3062.
- 43 E. R. Dufresne and D. G. Grier, *Rev. Sci. Instrum.*, 1998, **69**, 1974.
- 44 P. T. Korda, M. B. Taylor and D. G. Grier, *Phys. Rev. Lett.*, 2002, **89**, 128301.
- 45 J. P. Hoogenboom, D. L. J. Vossen, C. Faivre-Moskalenko, M. Dogterom and A. van Blaaderen, *Appl. Phys. Lett.*, 2002, **80**, 4828.
- 46 C. Mio and D. W. M. Marr, *Langmuir*, 1999, **15**, 8565.
- 47 G.-R. Yi, D. J. Pine and S. Sacanna, *J. Phys.: Condens. Matter*, 2013, **25**, 193101.
- 48 Z. Gong, T. Hueckel, G.-R. Yi and S. Sacanna, *Nature*, 2017, **550**, 234.
- 49 E. Bianchi, P. D. van Oostrum, C. N. Likos and G. Kahl, *Curr. Opin. Colloid Interface Sci.*, 2017, **30**, 8.
- 50 S.-M. Yang, S.-H. Kim, J.-M. Lim and G.-R. Yi, *J. Mater. Chem.*, 2008, **18**, 2177.
- 51 D. de las Heras, J. M. Tavares and M. M. Telo da Gama, *Soft Matter*, 2012, **8**, 1785.
- 52 F. Varrato, L. Di Michele, M. Belushkin, N. Dorsaz, S. H. Nathan, E. Eiser and G. Foffi, *Proc. Natl. Acad. Sci. U. S. A.*, 2012, **109**, 19155.
- 53 F. Seiferling, D. de las Heras and M. M. Telo da Gama, *J. Chem. Phys.*, 2016, **145**, 074903.
- 54 C. S. Dias, C. Braga, N. A. M. Araújo and M. M. Telo da Gama, *Soft Matter*, 2016, **12**, 1550.
- 55 C. S. Dias, N. A. M. Araújo and M. M. Telo da Gama, *J. Phys.: Condens. Matter*, 2018, **30**, 014001.